Exploiting Quality-Guided Adaptive Optimization for Fusing Multimodal Medical Images

LU TANG [1,2], **CHUANGENG TIAN** [3], **AND KAI XU** [2]
[1]School of Medical Imaging, Xuzhou Medical University, Xuzhou 221004, China
[2]Department of Radiology, Affiliated Hospital of Xuzhou Medical University, Xuzhou 221004, China
[3]School of Information and Electrical Engineering, Xuzhou University of Technology, Xuzhou 221004, China

Corresponding author: Kai Xu (xkpaper@163.com)

ABSTRACT Multimodal medical image fusion (MMIF) plays critical roles in image-guided clinical diagnostics and treatment. Pulse coupled neural network (PCNN) has been applied in image fusion for several years. In the schemes of image fusion based on PCNN, the authors have adjusted variables manually, so that it is difficult to get satisfying effects which limit in dealing with medical images with different modalities. This paper presents a quality-guided adaptive optimization method for MMIF, which is based on PCNN optimized by multi-swarm fruit fly optimization algorithm (MFOA). To reduce the implementation cost and improve the performance of the MFOA, quality assessment for multimodal medical image fusion was chosen to be the hybrid fitness function. Guided by such quality measurement, the adaptive PCNN using the MFOA (PCNN-MFOA) is proposed, which could automatically fit the optimal variables to the source images and enhance the fusion effect. The experimental results visually and quantitatively show that the proposed fusion strategy is more effective than the state-of-the-art methods and it is more effective in processing medical images with different modalities.

INDEX TERMS Quality guided, pulse coupled neural network, multi-swarm fruit fly optimization algorithm, multimodal medical image fusion.

I. INTRODUCTION

Image fusion integrates different sensory information into a visual enhanced representational format [1]–[3]. Fusion of multimodal medical images attracts much attention due to its critical role in clinical diagnostics and treatment. There are various modalities of medical images, which can be classified into anatomical and functional. Anatomical imaging modalities include x-ray computed tomography (CT), magnetic resonance imaging (MRI). For instance, CT image denote dense structures, but it is limited in soft tissue contrast. MRI can detect soft tissue. However, it cannot be used to provide bones and implants information [4]. Functional imaging modalities include single photon emission CT (SPECT) and positron emission CT (PET), which provide metabolic information without anatomical context like blood flow and flood activity with low spatial resolution. Single modality medical images may not enough to provide clinical

needs to radiologists [5]. Multimodal medical image fusion (MMIF) provides a promising solution approach by integrating information of different modality images into a visual enhanced fused images, it aids radiologists in significant clinical diagnosis [6], [7].

Up to now, many medical image fusion approaches have been presented. The most fusion methods are based on multiscale transform (MST) framework. The MST approaches can be divided into three steps. Firstly, source images are transformed to MST domain. Then, the MST coefficients are merged by designed fusion rulers. Finally, the fused image is obtained by the inverse transform. Classical MST-based fusion methods commonly include gradient pyramid [8], discrete wavelet transform [9], and contourlet transform [10], non-subsampled contourlet transform (NSCT) [11], non-subsampled shearlet transform (NSST) [12], and so on. To pursue encouraging fusion results, pulse coupled neural network (PCNN) are introduced under MST-based framework [13]–[16]. Such as, Huang et al. [14] used NSCT and PCNN for the fusion of

SPECT and CT images to improve the quality of fused brain images. However, authors did not consider other types of medical images. Jin et al. [15] proposed simplified PCNN based on non-subsampled shearlet transform (NSST-SPCNN) for multimodal sensor medical image fusion. Image pixel value is employed to stimulate the PCNN for processing high frequency coefficients. The coefficients with larger absolute values are fused into new low frequency coefficients. These methods were exploited on the basis of complementary strategies and thus achieve fairly high performance. However, in most cases, the PCNN parameters are set to constant based on adjusted manually through a great quantity of training, which hinders the performance of medical image fusion [16]. In simplified PCNN model, there are a few important parameters need to be set. A natural question is how to select the best parameters to conduct fusion. This is not an easy task, since defined parameters may produce the best quality on one pair input images, but it may be appropriate to the new input images not any longer. So, in most cases, researchers must try a great many times to find a suitable set of parameters based on different input images by empirical or experimental results. To a great extent, it may limit the robustness of algorithm performance. The adaptive optimization process of finding suitable parameters is similar to the optimization process of the intelligent optimization algorithm. MFOA is a global optimization approach, aiming to find the optimal solution search space by iteration. This motivates us to exploit a quality-guided adaptive optimization to automatically determine the optimal parameters for fusing multimodal medical images.

This paper proposes a quality-guided adaptive optimization method based on PCNN-MFOA. The main contributions of this paper are as follows.

1) We introduce a quality evaluation metric for MMIF (Q_{MMIF}) [17] as the quality-guided fitness function. In the process of search iteration, the design of the fitness function is the key. The fitness function needs to be used to evaluate the merits of the current position. The image objective evaluation index can measure the quality of the image and can be used as the basis for the fitness function selection. In addition, the Q_{MMIF} is experimentally proved to have more accurately than existing evaluation strategies in evaluating the MMIF image [17]. To the best of our knowledge, this is the first time that the Q_{MMIF} model is used as quality-guided adaptive optimization in the field of medical image fusion.

2) We first time propose an adaptive PCNN using the MFOA (PCNN-MFOA) model in the field of multimodal medical image fusion. The PCNN-MFOA model can overcome the difficulty of setting parameter-adaptive in the conventional PCNN models. The dynamic optimization of parameters is adjusted through the evaluation results, and the optimal variables can be automatically matched with the source image to obtain the optimal parameter combination.

3) We propose a new quality-guided adaptive optimization method for MMIF by applying the PCNN-MFOA mentioned earlier. Experiments are implemented to verify the effectiveness of proposed method on different imaging modalities of medical image. Representative MMIF algorithms are used as comparison experiments. Experimental results visually and quantitatively show that the proposed fusion strategy is more effective than state-of-the-art methods in processing medical images with different modalities.

The rest of this paper is organized as follows. In Section II, the theories of PCNN and MFOA are briefly introduced. Section III presents quality-guided PCNN-MFOA model and detailed fusion scheme. Experimental results and analysis are presented in Section IV. Finally, Section V gives conclusion.

II. RELATED WORKS
A. PULSE COUPLED NEURAL NETWORK
The schematic diagram of the simplified PCNN model is shown in FIGURE 1. There are three modules: the dendritic (feeding input $E_{u,v}$ and linking input $I_{u,v}(n)$), the linking modulation $M_{u,v}(n)$ and the pulse generator $F_{u,v}(n)$ [18], which are denoted by:

$$E_{u,v}(n) = S_{u,v} \tag{1}$$

$$I_{u,v}(n) = e^{-\alpha_L} I_{u,v}(n) + V_L \sum_{k,l} W_{u,v,k,l} F_{u,v}(n-1) \tag{2}$$

$$M_{u,v}(n) = E_{u,v}(n)\left[1 + \beta I_{u,v}(n)\right] \tag{3}$$

$$T_{u,v}(n) = e^{-\alpha_\theta} T_{u,v}(n-1) + V_\theta F_{u,v}(n-1) \tag{4}$$

$$F_{u,v}(n) = \begin{cases} 1, & M_{u,v}(n) > T_{u,v}(n) \\ 0, & M_{u,v}(n) \le T_{u,v}(n) \end{cases} \tag{5}$$
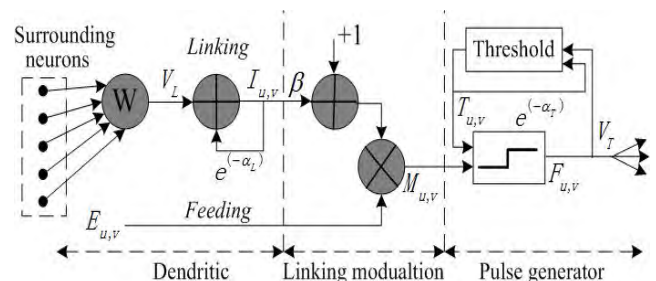

FIGURE 1. Schematic diagram of simplified PCNN.

where W is the synaptic weight matrices, u, v represent the pixel locations, k, l represent the dislocation in a symmetric neighbourhood surrounding a pixel. $S_{u,v}(n)$ is the external stimulus. In this paper, gray value of the pixel instead of external stimulus of PCNN. V_L and α_L represent normalizing constants. β is the linking parameter, which the weight of linking field. α_θ and V_θ denote attenuation coefficient and threshold magnitude coefficient, respectively.

B. MULTI-SWARM FRUIT FLY OPTIMIZATION ALGORITHM

Pan et al. [19] presented fruit fly optimization algorithm (FOA), aiming to hunt for global optimization automatically. It is as a simulation of intelligent foraging action of fruit flies hunting for food. The FOA metric affords us a useful design principle, and the program code is simple and easy to understand. However, this method tends to cause limiting in searching space. Furthermore, it is hard to get out of the local extremes [20]. Hence, the multi-swarm fruit fly optimization algorithm (MFOA) was presented by Yuan et al. [21]. It is a FOA-based approach, which employs multi-swarm action to significantly improve the performance. In the MFOA approach, the sub swarms divide by a huge swarm move independently searching space. Meantime, to searching global optimization at once, local search is done by cooperative sub-swarms, which is so far the complementation of MFOA close to the best values. The nonlinear equations with boundary conditions optimization question is depicted as follows:

$$\max f(Y) = f(y_1, y_2, \cdots, y_n), \quad y_j \in [a_j, b_j] \quad (6)$$

where $j \in \{1, 2, 3, \cdots n\}$, n is the number of decision variable. The detail of the MFOA is epitomized as following steps.

Firstly, fruit fly swarm location is initialized, which is denoted by *Init Y_axis*. The max iteration times are set k_{max}, population scale of fruit flies is *Popsize*, and sub swarms number is T. The individual fruit fly can use the smell to feed back its distance and direction to the food. The detailed implementation on each swarm is as follows:

$$Y_{i,t} = Y\_axis_t + R(k) \times Random \quad (7)$$

where $i \in \{1, 2, 3, \cdots Popsize\}$ denotes each fruit flies population, $t \in \{1, 2, 3, \cdots T\}$ denotes each sub swarm. $\phi \in [2, 6]$, $R(k)$ is denoted by

$$R(k) = \left(\frac{b_j - a_j}{2}\right) \times \left(\frac{k_{max} - k}{k_{max}}\right)^{\phi} \quad (8)$$

Secondly, in order to find fitness function value of the individual location of fruit fly, fitness function value ($Smell_i$) is substituted and denoted by decision variable value (Y_i). Best fitness function value among each sub-swarm is denoted by max (*smell*). They are listed as follows:

$$Smell_i = Function(Y_i)$$
$$[bestSmell_t \; bestIndex_t] = \max(Smell) \quad (9)$$

When the fitness of each sub swarm is better than the prior iteration fitness, the optimum fitness is updated, meantime, each sub swarm will fly to that location on one's own with sense of sight, which are listed as follows:

$$Smellbest_t = bestSmell_t$$
$$Y\_axis_t = Y(bestIndex_t) \quad (10)$$

Next, the global fitness and best position are updated, which are denoted by *Smellbest* and *Y_axis*, respectively.

If the $Smellbest_t > Smellbest$, the $Smellbest = Smellbest_t$, $Y\_axis = Y\_axis_t$. Cooperative local search is conducted by

$$Y\_new = \frac{1}{T} \sum_{t=1}^{T} X\_axis_t \quad (11)$$

when $Function(Y_{new}) > Smellbest$, the global fitness and best position are updated and denoted by

$$Smellbest = Function(Y\_new)$$
$$Y\_axis = Y\_new \quad (12)$$

Finally, if $k \geq k_{max}$, then, iteration stops.

III. MULTIMODAL MEDICAL IMAGES FUSION STRATEGY

A. THE QUALITY-GUIDED FITNESS FUNCTION

In order to solve the optimal parameters of the PCNN, the intelligent optimization algorithm MFOA was used to optimize the parameters of the PCNN. In the process of search iteration, the fitness function needs to be used to evaluate the merits of the current position. Therefore, the design of the fitness function is the key. A natural problem is how to select the appropriate evaluation criteria to construct the fitness function. The fitness function is an important factor affecting the search performance of the MFOA. The image objective evaluation index can measure the quality of the image and can be used as the basis for the fitness function selection. Many image quality assessment approaches have been presented [22]–[24], however these existing evaluation criterias are not designed for MMIF, which limit in evaluating multimodal fused images, and little has been done to compare them with subjective data that contains a wide variety of image modalities and fusion algorithms. In our previous work [17], a MMIF image database is built, 20 radiologists participated in the subjective test, the proposed quality evaluation metric for MMIF (Q_{MMIF}) can maintain good consistency with the subjective experimental results, and can more accurately evaluate the MMIF image. In this paper, the fitness function is constructed by the Q_{MMIF} evaluation criterion, which advances fruit flies to fly from the original location to the best location with higher effectiveness. Guided the quality assessment, adaptive PCNN model using the MFOA (PCNN-MFOA) are constructed, which is determined according to the fitness function. The dynamic optimization of the parameters is adjusted through the evaluation results, and the optimal variables can be automatically matched with the source image to obtain the optimal parameter combination. Hence, a evaluation criterion for MMIF fitness function is computed and denoted by

$$Smellbest = Q_{MMIF} \quad (13)$$

B. PCNN-MFOA

In simplified PCNN model, several parameters are very important in affecting the performance of PCNN model. Attenuation time constant α_L determines the attenuation speeds of the L-channel. Decay time constant α_θ regulates
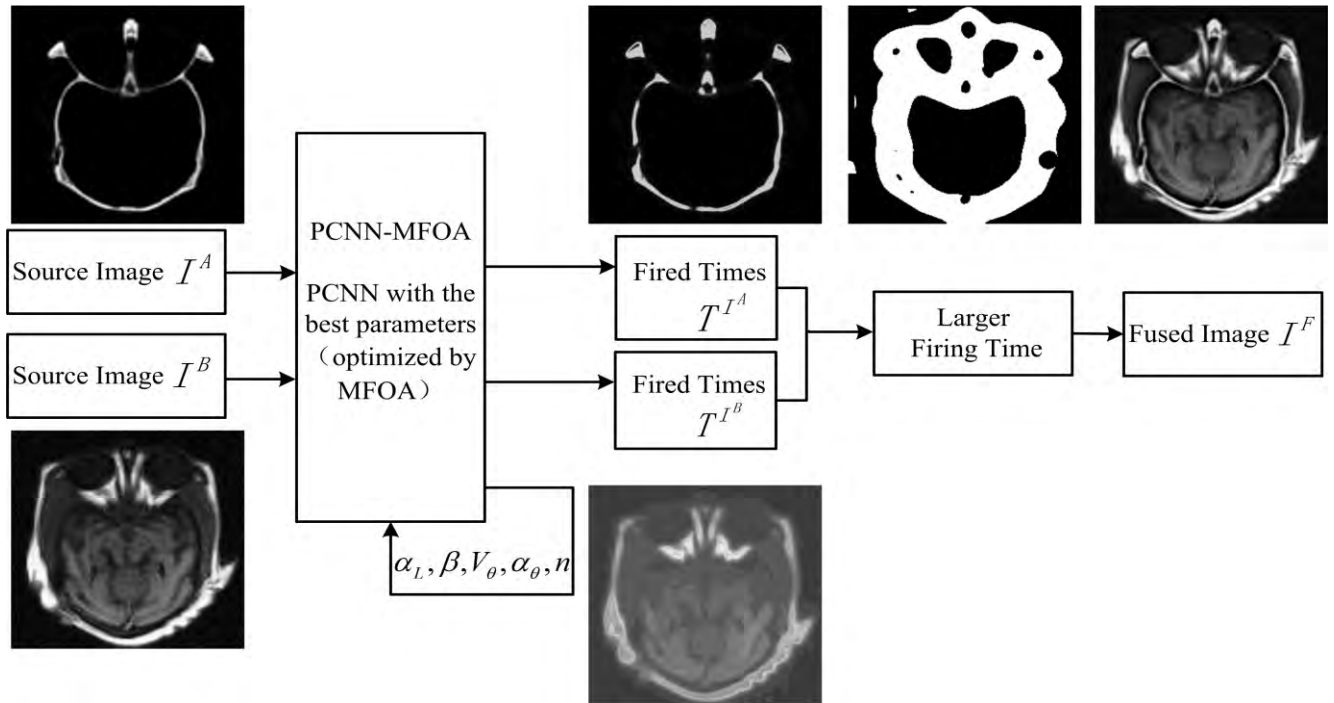
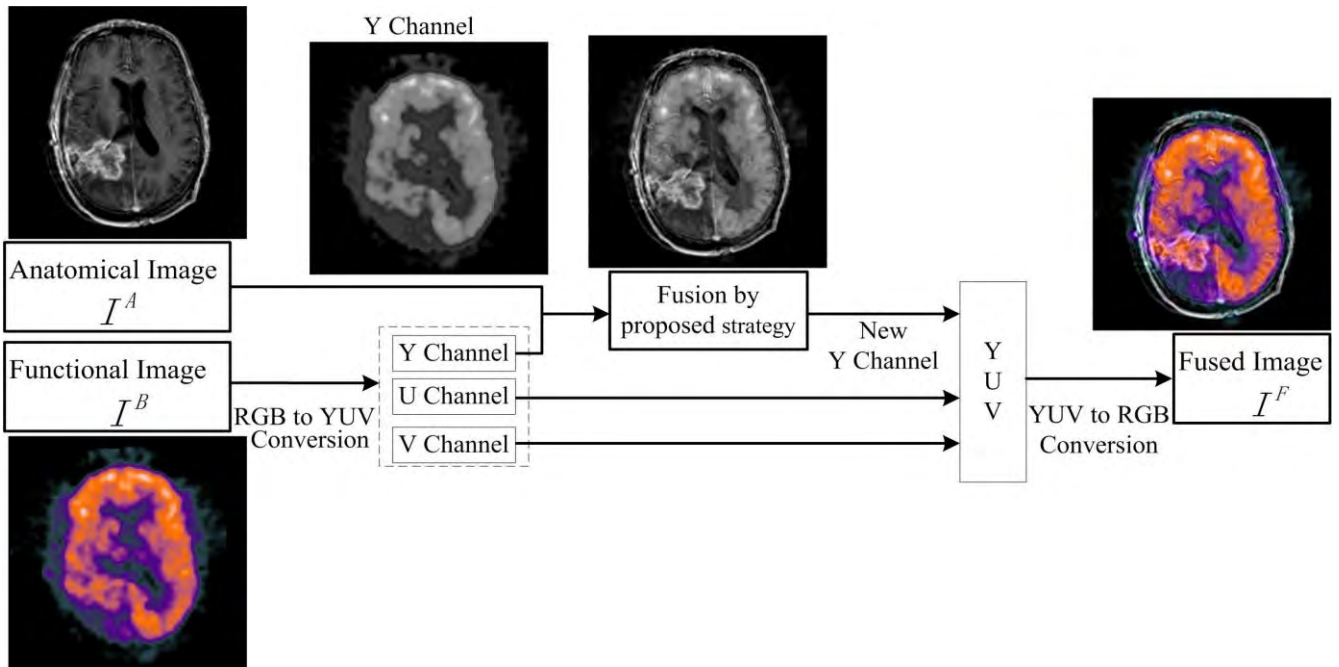**FIGURE 2.** Schematic diagram of PCNN-MFOA fusion strategy.

FIGURE 3. Schematic of the grayscale and color image fusion strategy.

the decline rate of the threshold value, and the threshold decreases slower and the more times the PCNN employs if the value is smaller. The threshold amplitude coefficient V_θ regulates the neuron firing cycle, once a neuron fires, its amplitude exceeds the threshold and will be promoted. The link strength coefficient β adjusts the extent to which neighboring neurons affect central neurons. The large β causes widespread

pulse synchronization. Iteration number n can not only reduce the computational complexity, but also increase the computing speed of the PCNN.

Considering the above reasons, these five important parameters ($\alpha_L, \beta, V_\theta, \alpha_\theta, n$) need to be determined. The sub-swarms number of the fruit flies represents the number of parameters, so the sub-swarms number is 5, the size of population is

Algorithm 1 Procedures of PCNN-MFOA

Input: k_{max}, *Popsize*, T, n, image I^A, image I^B
For t = 1:T
   For j =1: n
      Initialization Y_axis_t
   End for
End for
For k = 1: k_{max}
   For i = 1: *Popsize*
      For t = 1:T
         $Y_{it} = Y\_axis_t + R(k) \times Random$
      End for
      $F_i = fused$ (image I^A, image I^B, Y_i)
      $Smell_i = Function(Y_i) = Q_{MMIF}(F_i)$
   End for
   $[bestSmell_t \ bestIndex_t] = max(Smell)$
   $Smellbest_t = bestSmell_t$
   $Y\_axis_t = Y(bestIndex_t)$
   If $Smellbest_t > Smellbest$
      $Smellbest = Smellbest_t$
      $Y\_axis = Y\_axis_t$
   End If
   $Y\_new = \frac{1}{T} \sum_{t=1}^{T} Y\_axis_t$
   $F = fused$ (image I^A, image I^B, Y_new)
   $Smell\_new = Function(Y\_new)$
   If $Function(Y\_new) > Smellbest$
      $Smellbest = Function(Y\_new)$
      $Y\_axis = Y\_new$
   End If
End for
Output: $Smellbest$, $Y\_axis \left((\alpha_L, \beta, V_\theta, \alpha_\theta, n) \right.$
Output, $Y\_axis \left(\alpha_L, \overline{\beta}, V_\theta, \alpha_\theta, n \right)$

set to 20, and the terminal condition exceeding the maximal iterations number will be not executed. The detailed of the proposed PCNN-MFOA are shown as Algorithm 1.

C. FUSION STRATEGY BASED ON PCNN-MFOA

Schematic diagram of the fusion strategy based on PCNN-MFOA is shown in FIGURE 2. Uniformly, medical image I^A and medical image I^B denote two source images with different modalities, let I^F denote the fused image. The detailed fusion scheme is summarized as following steps.

Firstly, image I^A and image I^B are conducted based on PCNN-MFOA, the optimal parameters are calculated according to Algorithm 1.

$$(\alpha_L, \beta, V_\theta, \alpha_\theta, n) = PCNN - MFOA \left(I^A \right)$$

$$(\alpha_L, \beta, V_\theta, \alpha_\theta, n) = PCNN - MFOA \left(I^B \right) \quad (14)$$

where PCNN-MFOA($\cdot$) denotes the PCNN-MFOA functions, which was described in section III. B.
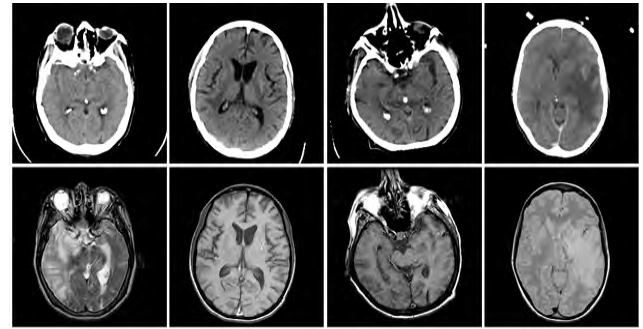
(G1) CT and MRI
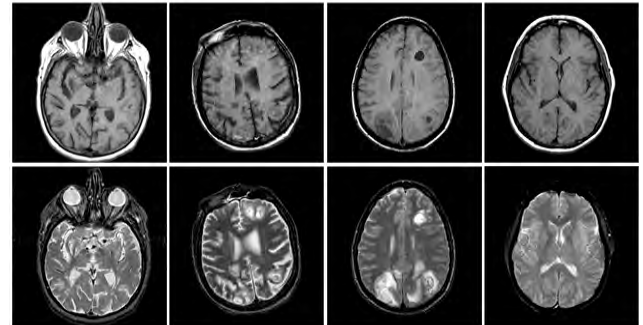
(G2) MRI-T1 and MRI-T2
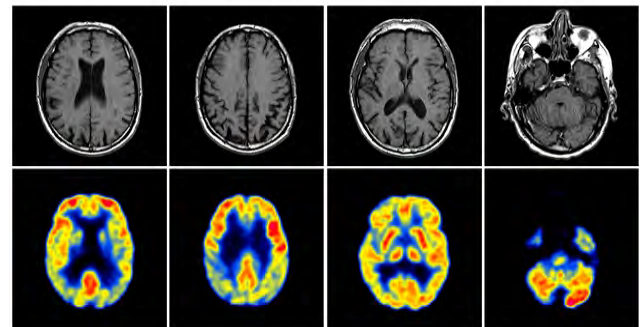
(G3) MRI and PET
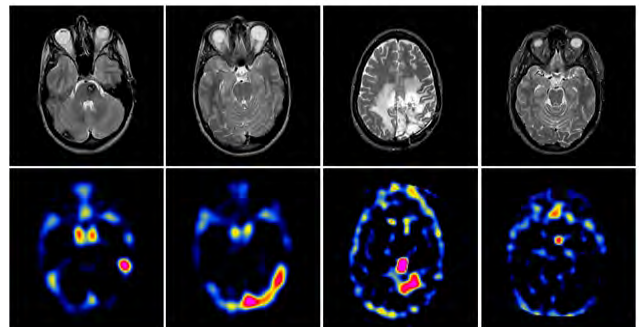
(G4) MRI and SPECT

FIGURE 4. Source multimodal medical images.

Secondly, the $I^A(u,v)$ and $I^B(u,v)$ are used as the stimulus of the PCNN for processing I^A and I^B, respectively.

$$T^{I^A} = PCNN \left(I^A(u, v) \right)$$

$$T^{I^B} = PCNN \left(I^B(u, v) \right) \quad (15)$$
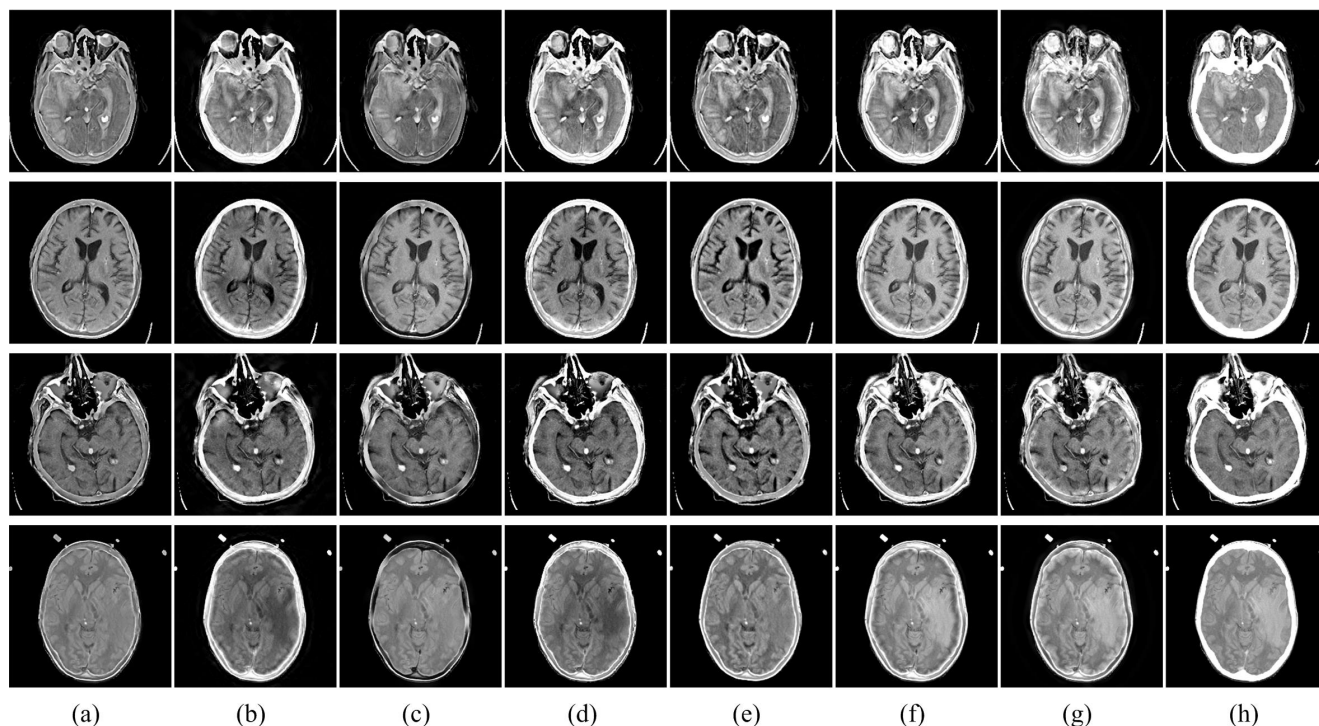
FIGURE 5. Four experimental results for CT and MR image fusion with eight methods (a) CSR. (b) NSCT-PCNN-SF. (c) GFF. (d) LP-SR. (e) ULAP-MF. (f) NF. (g) NSST-PAPCNN. (h) Proposed.
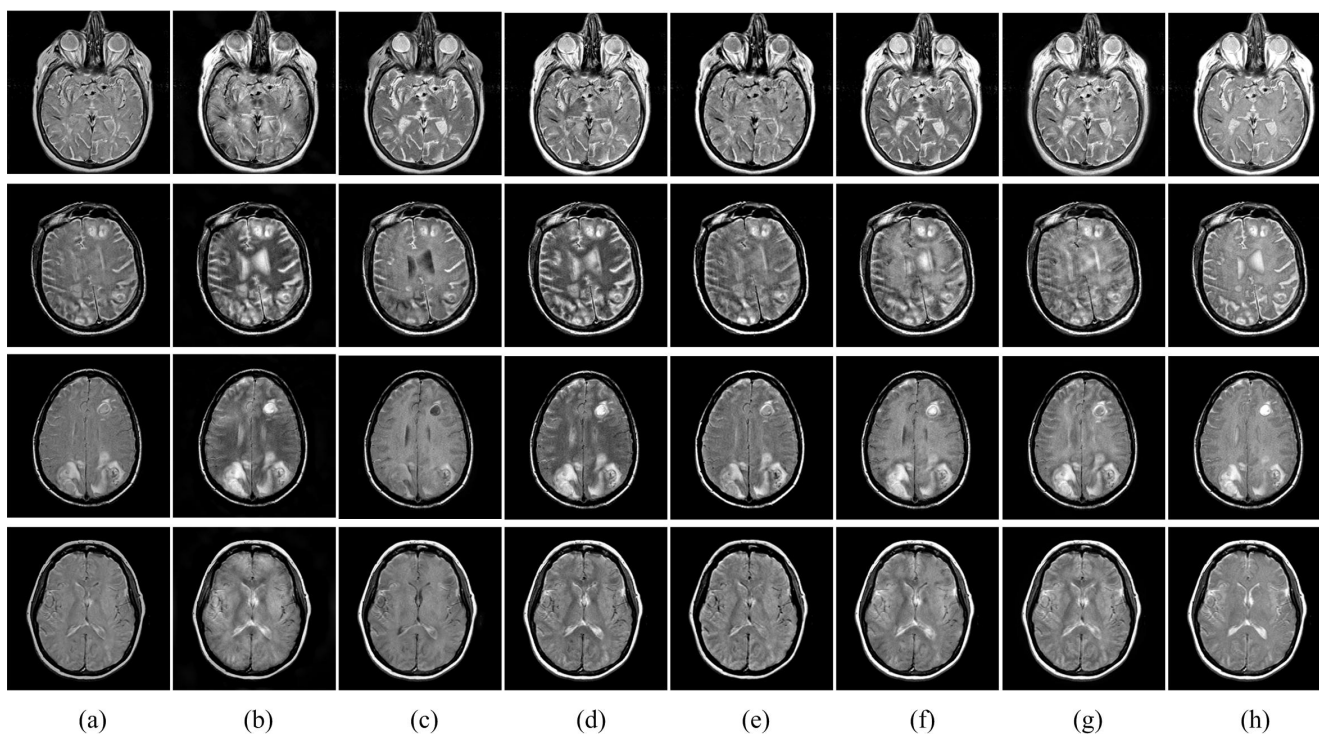
FIGURE 6. Four experimental results for MR-T1 and MR-T2 image fusion with eight methods (a) CSR. (b) NSCT-PCNN-SF. (c) GFF. (d) LP-SR. (e) ULAP-MF. (f) NF. (g) NSST-PAPCNN. (h) Proposed.

where PCNN($\cdot$) denotes the best parameters ($\alpha_L, \beta, V_\theta, \alpha_\theta, n$) by Eqs. (1)-(5). The firing times matrix T^{I^A} and T^{I^B} denote the total fired times motivated by $I^A(u,v)$ and $I^B(u,v)$, respectively. When the iteration number $n = k_{max}$, k_{max} is the max iteration times, then iteration stops.

FIGURE 7. Four experimental results for MR and PET image fusion with eight methods. (a) CSR. (b) NSCT-PCNN-SF. (c) ULAP-MF. (d) NF. (e) NSST-PAPCNN. (f) LLF-II. (g)PSF. (h) Proposed.
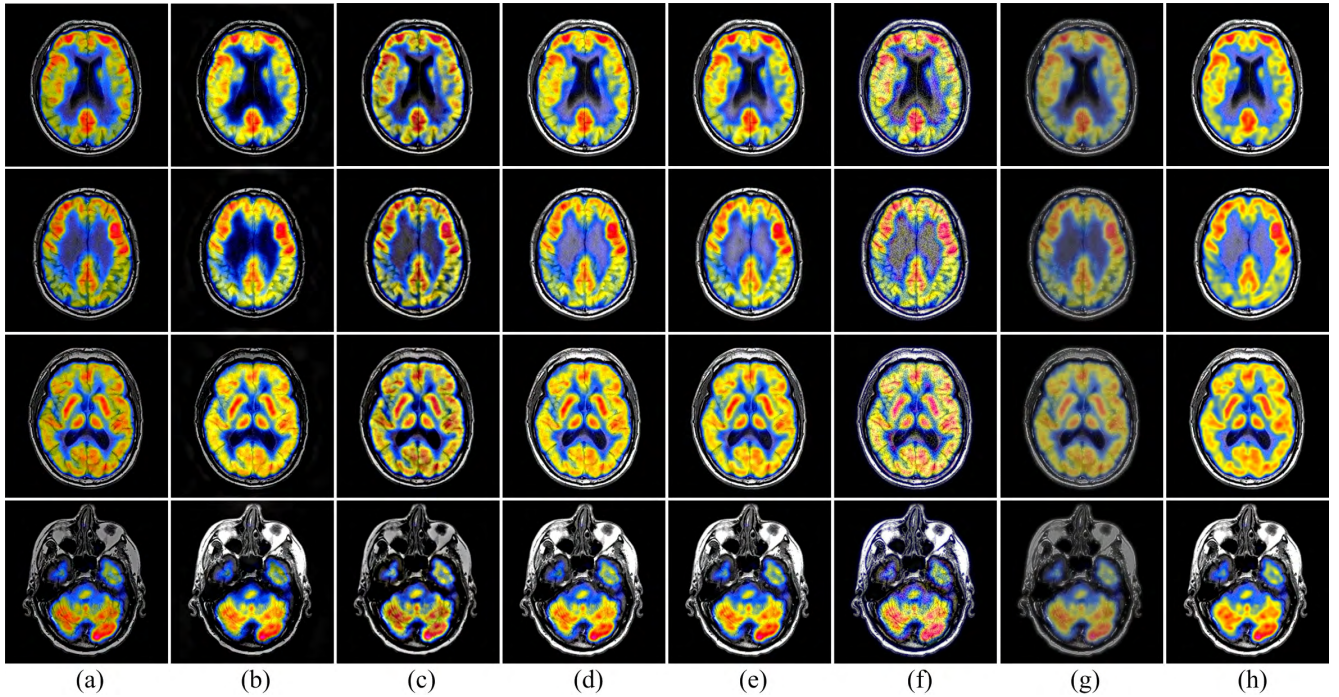
Finally, I^F is computed and denoted as follows:

$$
I^F = \begin{cases} \max\left(I^A(u,v), I^B(u,v)\right) & T^{I^A} = T^{I^B} \\ I^A(u,v) & T^{I^A} > T^{I^B} \\ I^B(u,v) & T^{I^A} < T^{I^B} \end{cases} \quad (16)
$$

D. EXTENSION TO ANATOMICAL AND FUNCTIONAL IMAGE FUSION

In this subsection, the proposed method is extended to fuse anatomical images and functional images. In medical imaging modalities, functional images (e.g., PET and SPECT) are pseudocolor images. The color space transform can divide color image into luminance or brightness component, especially, the YUV color space transform method have proved a very effective way for anatomical and functional image fusion [13], [16], [25]. This paper apply YUV color space transform to separate a color image into one luminance component (Y) and two chrominance components (U and V). Schematic diagram of the anatomical and functional image fusion strategy is shown in FIGURE 3. Specifically, the fusion scheme is outlined as following:

Firstly, the RGB image is transformed into YUV color space with three channels of Y, U, and V. The RGB to YUV color space conversion can be denoted by

$$
\begin{bmatrix} Y \\ U \\ V \end{bmatrix} = \begin{bmatrix} 0.299 & 0.587 & 0.114 \\ -0.169 & -0.331 & 0.5 \\ 0.5 & -0.419 & -0.081 \end{bmatrix} \begin{bmatrix} R \\ G \\ B \end{bmatrix} \quad (17)
$$

Then, fused Y channel (new Y channel) is obtained by the grayscale image and the Y channel fusion

based on the proposed fusion strategy, which described in section III. C.

Next, the new YUV are obtained by combining fused Y channel, the original U channel, and the original V channel.

Finally, the fused color image is contructed by inverse YUV transform. YUV to RGB space is computered by the following inverse operations:

$$
\begin{bmatrix} R \\ G \\ B \end{bmatrix} = \begin{bmatrix} 1 & 0 & 1.14 \\ 1 & -0.39 & 0.58 \\ 1 & 2.03 & 0 \end{bmatrix} \begin{bmatrix} Y \\ U \\ V \end{bmatrix}. \quad (18)
$$

IV. EXPERIMENTAL RESULTS

A. EXPERIMENTAL SETTINGS

In this subsection, four groups of medical images with size 256×256 are performed as shown in FIGURE 4. They are CT and MRI, MRI-T1 and MRI-T2, MRI and PET, MRI and SPECT. For each group, four sets of images are employed in the experiments, and the two source images should be preregistered.

To evaluate the effectiveness of the PCNN-MFOA strategy, the following fusion algorithms are used as comparison experiments, including convolutional sparse representation (CSR) [26], NSCT and PCNN with modified spatial frequency (NSCT-PCNN-SF) [13], guided filtering (GFF) [27], laplace transform and sparse representation (LP-SR) [28], union laplacian pyramid with multiple features (ULP-MF) [29], neuro-fuzzy (NF) [30], parameter-adaptive PCNN in NSST (NSST-PAPCNN) [16], local laplacian
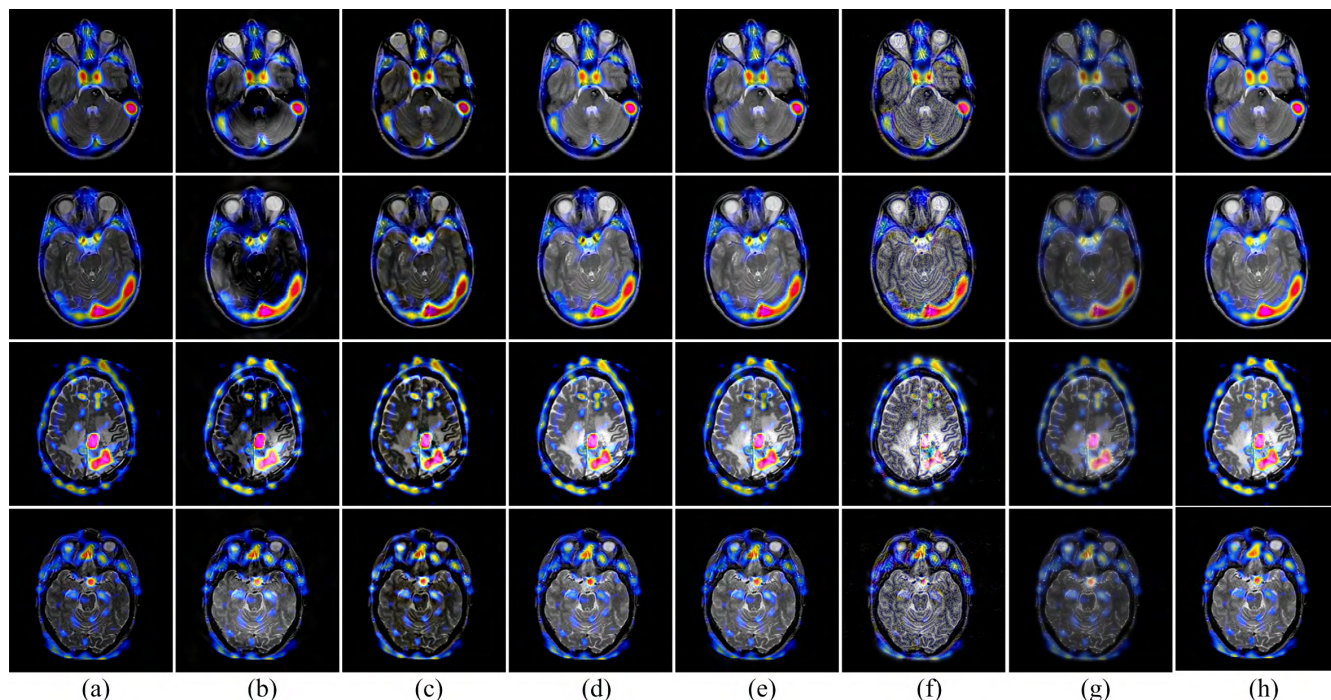
FIGURE 8. Four experimental results for MR and SPECT image fusion with eight methods. (a) CSR. (b) NSCT-PCNN-SF. (c) ULAP-MF. (d) NF. (e) NSST-PAPCNN. (f) LLF-II. (g)PSF. (h) Proposed.

TABLE 1. Objective assessment of the proposed methods with different fitness function.

Metric	fitness function(SD)	fitness function (MI)	fitness function (Q_G)	fitness function (Q_Y)	fitness function (Q_{MMIF})
SD	76.41	75.01	75.31	74.96	**76.72**
MI	1.19	1.20	1.17	1.18	**1.22**
Q_G	0.81	0.80	0.82	0.79	**0.83**
Q_Y	0.56	0.55	0.57	0.57	**0.58**

filtering and information of interest (LLF-II) [31], parallel saliency features (PSF) [32], where GFF, LP-SR are generally used to fuse anatomical- anatomical image, LLF-II, PSF are specifically for anatomical-functional image, CSR, NSCT-PCNN-SF, ULP-MF, NF, NSST-PAPCNN are used not only to fuse anatomical-anatomical image, but also to fuse anatomical-functional image. Among the nine compared methods, all the parameters are default values in implementation. The choice of fitness function is determined by experiments. In implementation, the fitness function is constructed by the standard deviation (SD) [28], the normalized mutual information (MI) [33], Xydeas et al.'s gradient based metric Q_G [34], Yang et al.'s metric (Q_Y) [35], and Q_{MMIF} [17], respectively, in MMIF image database [17]. We find the results of Q_{MMIF} in objective evaluation metrics are best. As shown in the TABLE 1, each value is the average result of all the source images, and the highest values are labeled in bold, which denote the best performance. In the experiment, we calculate the total running time of fusing all 16 pairs of source images, and then divide it by 16 to get the average running time, and repeated 10 times. The average running time is 136.56 seconds, iteration times are

20, and the optimized iteration time is 6.83 seconds. An experienced radiologist participated in subjective visual quality evaluation in terms of the proposed method. For each image set, the radiologist was asked to give results to each fused image within a continuous range, which can obtain more accurate subjective evaluation. He believed that the images fused by our proposed method preserve more edge, details and texture information, and have higher contrast and sharpness than source images, which is useful in diagnoses for doctors.

B. VISUAL QUALITY ANALYSIS

FIGURE 5 shows four experimental results for CT and MR image fusion with eight methods. It can be seen that images fused by CSR, GFF, LP-SR, ULAP-MF, NF, NSST-PAPCNN methods lose bone information. Among the CSR, GFF, ULAP-MF, NSST-PAPCNN methods, bone information are invisible [see the bone regions in FIGURE 5(a), (c), (e) and (g)]. The LP-SR and NF methods obtain part of skeleton information [see the bone regions in FIGURE 5(d), (f)]. NSCT-PCNN-SF method conserve better

TABLE 2. Objective assessment for CT and MRI.

Metric	CSR	NSCT-PCNN-SF	GFF	LP-SR	ULAP-MF	NF	NSST-PAPCNN	Proposed
SD	77.3536	84.7393	74.7308	87.6290	83.5038	92.7919	92.4223	**100.4384**
MI	0.6375	0.5198	0.6173	0.6828	0.5934	0.6857	0.6066	**1.1709**
Q_G	0.7102	0.4185	0.6854	0.7336	0.6714	0.6914	0.5946	**0.7409**
Q_Y	0.4298	0.3751	0.4507	0.4359	0.3646	0.4352	0.4285	**0.4962**
SD	69.2032	76.6673	72.4692	78.4381	76.9331	86.5513	84.3841	**90.6432**
MI	0.6766	0.6405	0.7229	0.7104	0.6128	0.7677	0.6187	**1.2487**
Q_G	0.6945	0.3796	0.7165	0.7318	0.6700	0.6922	0.5719	**0.7625**
Q_Y	0.4402	0.4039	0.4902	0.4385	0.3659	0.4540	0.4239	**0.5286**
SD	65.4763	75.0967	67.1198	80.6568	72.4710	85.0413	80.7258	**91.1594**
MI	0.5615	0.4757	0.5669	0.6089	0.5293	0.6325	0.5300	**1.1204**
Q_G	0.6518	0.3720	0.6760	0.6750	0.6094	0.6793	0.5855	**0.7501**
Q_Y	0.5011	0.4348	0.5386	0.5115	0.4150	0.5386	0.4951	**0.5979**
SD	66.4225	71.8582	66.6633	70.0952	72.8595	82.1165	80.3479	**88.0977**
MI	0.7121	0.6921	0.7204	0.7621	0.7127	0.7983	0.6374	**1.3339**
Q_G	0.6866	0.3645	0.7139	0.7408	0.6894	0.7108	0.5749	**0.7877**
Q_Y	0.3925	0.3477	0.4331	0.3982	0.3401	0.3942	0.3843	**0.4887**

TABLE 3. Objective assessment for MRI-T1 and MRI-T2.

Metric	CSR	NSCT-PCNN-SF	GFF	LP-SR	ULAP-MF	NF	NSST-PAPCNN	Proposed
SD	68.8739	75.6272	71.8232	80.8769	77.2804	82.4238	80.6689	**87.5877**
MI	0.5826	0.4757	0.6779	0.6009	0.5159	0.6962	0.5380	**1.1449**
Q_G	0.6135	0.4178	0.6878	0.6773	0.5247	0.6906	0.5545	**0.7435**
Q_Y	0.6473	0.5555	0.7362	0.7191	0.5476	0.7484	0.6350	**0.7808**
SD	58.8539	62.4569	63.5591	64.6256	64.4716	68.3140	68.2900	**73.8038**
MI	0.7263	0.6119	0.74592	0.7662	0.6310	0.7460	0.6526	**1.2406**
Q_G	0.7155	0.5116	0.7397	0.7635	0.6393	0.7214	0.6198	**0.8150**
Q_Y	0.4596	0.4571	0.5048	0.5071	0.3765	0.4753	0.4271	**0.5344**
SD	59.2213	59.8697	62.4578	60.5977	64.3417	67.7925	67.5734	**70.5352**
MI	0.7604	0.6621	0.8529	0.8070	0.6909	0.8410	0.7083	**1.2698**
Q_G	0.7145	0.4779	0.7508	0.7457	0.6659	0.7494	0.6466	**0.8174**
Q_Y	0.4219	0.4031	0.4704	0.4342	0.3441	0.4589	0.4080	**0.4840**
SD	61.5714	66.9841	66.3428	68.1068	67.9644	71.3403	71.7129	**74.1155**
MI	0.70374	0.5655	0.7390	0.7358	0.6441	0.7486	0.6956	**1.2236**
Q_G	0.70394	0.4736	0.7548	0.7480	0.6497	0.7261	0.6497	**0.8092**
Q_Y	0.43274	0.3997	0.4996	0.4794	0.3809	0.4573	0.4832	**0.5225**

effect on this issue, but still lead to some edge skeleton structures blurring, and some details lose and the contrast of the focal lesions decrease [see the bone regions and focal regions in FIGURE 5(b)]. Our method achieves better results on bone information preservation and detail extraction [see FIGURE 5(h)].

FIGURE 6 shows four experimental results for MR-T1 and MR-T2 image fusion. The CSR, GFF, ULAP-MF, NF, NSST-PAPCNN methods are not successful in extracting the detail structure from the MR-T2 image. The CSR, GFF methods lead to the details of MR-T2 image almost invisible [see FIGURE 6(a), (c)], the ULAP-MF, NF, NSST-PAPCNN

methods obtain part MR-T2 details, but some details are still serious loss [see the focal regions and cerebrospinal fluid region in FIGURE 6(e), (f) and (g)]. The NSCT-PCNN-SF and LP-SR methods perform well, some regions cause intensity and contrast decrease, leading to a significant structure blur in gray and white matter region [FIGURE 6(b), (d)]. The proposed method achieve well in all these four examples.

FIGURE 7 shows four experimental results for MR and PET image fusion with eight methods. The LLF-II method introduces serious noise like artifacts in fused image [see FIGURE 7(f)]. The PSF method leads to whole image blur

TABLE 4. Objective assessment for MRI and PET.

Metric	CSR	NSCT-PCNN-SF	ULAP-MF	NF	NSST-PAPCNN	LLF-II	PSF	Proposed
SD	59.8627	71.6602	67.9561	76.4802	75.5809	75.7862	58.6945	**77.9129**
MI	0.67607	0.5373	0.5950	0.7697	0.6573	0.6310	0.6133	**1.2562**
Q_G	0.75957	0.4767	0.6909	0.8005	0.7195	0.6868	0.5936	**0.8535**
Q_Y	0.4167	0.3412	0.3514	0.4623	0.4523	0.3970	0.3241	**0.5214**
SD	56.4368	69.2150	63.7446	75.2991	74.5749	74.5685	55.7497	**76.4959**
MI	0.6891	0.5235	0.6311	0.7577	0.6511	0.6426	0.6235	**1.2583**
Q_G	0.7790	0.4848	0.7196	0.8080	0.7319	0.7120	0.6188	**0.8512**
Q_Y	0.3790	0.3111	0.3307	0.4139	0.4023	0.3613	0.2826	**0.4786**
SD	64.3636	77.8214	72.7058	82.8465	82.0254	82.5021	63.2163	**83.9438**
MI	0.6436	0.5320	0.5656	0.7527	0.6529	0.6151	0.5825	**1.2560**
Q_G	0.7616	0.4681	0.6778	0.7981	0.7272	0.6848	0.5786	**0.8426**
Q_Y	0.4504	0.3692	0.3768	0.4870	0.4781	0.4249	0.3505	**0.5496**
SD	52.9306	71.3578	61.9165	75.4502	75.4842	74.4286	50.4292	**76.0762**
MI	0.5952	0.5317	0.5201	0.8790	0.8025	0.6097	0.5186	**1.2263**
Q_G	0.7801	0.6263	0.6752	0.8735	0.8576	0.7413	0.5612	**0.9180**
Q_Y	0.4411	0.4461	0.3681	0.5447	0.5355	0.4839	0.3483	**0.5751**

TABLE 5. Objective assessment for MRI and SPECT.

Metric	CSR	NSCT-PCNN-SF	ULAP-MF	NF	NSST-PAPCNN	LLF-II	PSF	Proposed
SD	35.3904	46.0798	41.3799	54.8497	54.3450	54.2970	35.2618	**55.7796**
MI	0.5698	0.3651	0.4841	0.8235	0.6655	0.5575	0.5524	**1.2088**
Q_G	0.8131	0.5776	0.7259	0.8852	0.8477	0.7226	0.6199	**0.9190**
Q_Y	0.3783	0.3591	0.3243	0.4728	0.4616	0.3803	0.2832	**0.4914**
SD	38.5251	45.2876	43.6933	58.4998	58.3182	58.5761	38.6656	**59.8486**
MI	0.5652	0.3094	0.4864	0.8311	0.6751	0.5531	0.5473	**1.19401**
Q_G	0.8197	0.5150	0.7194	0.8825	0.8402	0.7080	0.6005	**0.9103**
Q_Y	0.4096	0.3185	0.3471	0.5005	0.4917	0.4035	0.3005	**0.5140**
SD	45.8440	51.0417	52.1111	67.9623	66.4921	66.9061	45.8247	**69.0397**
MI	0.5572	0.3915	0.4727	0.7266	0.5590	0.5097	0.5057	**1.2003**
Q_G	0.6890	0.5038	0.6177	0.7988	0.7163	0.6065	0.5016	**0.9067**
Q_Y	0.6095	0.4452	0.5569	0.7528	0.6679	0.5492	0.5373	**0.8331**
SD	33.7018	47.9743	38.9038	51.2749	50.5298	51.2909	33.9306	**52.0737**
MI	0.5502	0.4116	0.4478	0.7988	0.6541	0.5312	0.4934	**1.1698**
Q_G	0.6917	0.5654	0.5823	0.8158	0.8129	0.6440	0.4862	**0.9159**
Q_Y	0.6289	0.5651	0.5663	0.7870	0.7808	0.6060	0.5627	**0.8594**

[see FIGURE 7(g)]. The NSCT-PCNN-SF method suffers from important anatomical information of MR source image lost [see FIGURE 7(b)]. The CSR, ULAP-MF methods cause severe color distortion [cerebral metabolism regions in see FIGURE 7(a), (c)]. The NF, NSST-PAPCNN methods perform better on this issue, but fails in preserving color fidelity. In addition, unclosure or incontinuity effects exist more or less in the fused images, which lead to some important functional information of PET image lost [see cerebral metabolism regions in FIGURE 7(d), (e)]. Compared with the above methods, our method achieves the best visual performance [see FIGURE 7(h)].

FIGURE 8 shows four experimental results for MR and SPECT image fusion with eight methods. It can be clearly seen that the image fused by LLF-II suffers from serious noise like artifacts [see FIGURE 8(f)]. The PSF method fails in preserving image sharpness [see the serious visual blur in whole image regions in FIGURE 8(g)]. The main defect of CSR, NSCT-PCNN-SF, ULAP-MF method is not successful in preserving intensity and contrast, leading to important anatomical information in MR source image lost [see the gray and white matter regions in FIGURE 8(a), (b), (c).] In addition, color information blur or even lost exists more or less in the fused images [see hypermetabolism regions in

FIGURE 8(a), (b), (c)]. The NF, NSST-PAPCNN methods obtain better fusion results, but fails in obtaining important functional information of SPECT source image, because it over enhances the anatomical details in the MR source images [see abnormal metabolites regions in FIGURE 8 (d), (e)]. The proposed strategy preserves edge, details, texture information, and metabolic information [see FIGURE 8 (h)].

C. OBJECTIVE QUALITY ASSESSMENT

Objective quality assessment plays an important role in image fusion filed. Recently, many fusion metrics have been proposed, one question to how to select the best criteria to measure the fused image quality. This is not an easy task, since perfect reference images (ground truth) are usually unavailable in the real world medical imaging. So far, a few of approaches have been presented for the quality measurement of the fused images. In this work, four fusion quality metrics are adopted, which are SD [28], MI [33], Q_G [34], Q_Y [35]. SD measures the contrast in the fused image. MI measures the amount of information transferred to the fused image from the source images. Q_G evaluates the success of edge information or gradient information from source images is injected in to the fused image from the source images. Q_Y utilizes the structure similarity to measure the structural information between the fused image and each source image. In general, the larger the values of SD, MI, Q_G, and Q_Y denote better fusion quality. TABLE 2-5 summarizes the objective assessment performance of our method and existing methods employing the above four metrics, where the highest score values are marked boldfaced in each row, which denote the best results. From the TABLE 2-5, it is clear that our method achieves the significant superiority.

V. CONCLUSION

In this paper, we have presented a quality-guided adaptive optimization method for fusing multimodal medical images. Guided by quality measurement, PCNN-MFOA is proposed, which could automatically determine the optimal parameters for source images, and deal with medical images with different modalities. Extensive experimental results demonstrate that the proposed fusion strategy has much higher performance than the state-of-the-art methods. Furthermore, the proposed method is very helpful for the radiologists in clinical application.

REFERENCES

[1] Y. Yang, L. Wu, S. Huang, W. Wan, and Y. Que, "Remote sensing image fusion based on adaptively weighted joint detail injection," *IEEE Access*, vol. 6, pp. 6849–6864, 2018.

[2] Y. Tong and J. Chen, "Multi-focus image fusion algorithm in sensor networks," *IEEE Access*, vol. 6, pp. 46794–46800, 2018.

[3] S. Choi, O.-J. Kwon, and J. Lee, "A method for fast multi-exposure image fusion," *IEEE Access*, vol. 5, pp. 7371–7380, 2017.

[4] L. Tang, J. S. Qian, L. Li, J. Hu, and X. Wu, "Multimodal medical image fusion based on discrete Tchebichef moments and pulse coupled neural network," *Int. J. Imag. Syst. Technol.*, vol. 27, no. 1, pp. 57–65, Jan. 2017.

[5] J. Qian, B. Rong, W. Shen, J. Hu, L. Tang, and Z. Xia, "Perceptual medical image fusion with internal generative mechanism," *Electron. Lett.*, vol. 53, no. 17, pp. 1184–1186, Aug. 2017.

[6] R. C. Krempien, S. Daeuber, F. W. Hensley, M. Wannenmacher, and W. Harms, "Image fusion of CT and MRI data enables improved target volume definition in 3D-brachytherapy treatment planning," *Brachytherapy*, vol. 2, no. 3, pp. 164–171, 2003.

[7] A. C. Paulino, W. L. Thorstad, and T. Fox, "Role of fusion in radiotherapy treatment planning," *Seminars Nucl. Med.*, vol. 33, no. 3, pp. 238–243, Jul. 2003.

[8] V. S. Petrovic and C. S. Xydeas, "Gradient-based multiresolution image fusion," *IEEE Trans. Image Process.*, vol. 13, no. 2, pp. 228–237, Feb. 2004.

[9] M. P. Kumar and R. P. Kumar, "Enhancing bio-medical mammography image fusion using optimized genetic algorithm," *J. Med. Imag. Health Inform.*, vol. 9, no. 3, pp. 502–507, Mar. 2019.

[10] L. Yang, B. L. Guo, and W. Ni, "Multimodality medical image fusion based on multiscale geometric analysis of contourlet transform," *Neurocomputing*, vol. 72, nos. 1–3, pp. 203–211, Dec. 2008.

[11] Y. Yang, S. Tong, S. Huang, and P. Lin, "Log-Gabor energy based multimodal medical image fusion in NSCT domain," *Comput. Math. Methods Med.*, vol. 2014, Aug. 2014, Art. no. 835481.

[12] C. S. Asha, S. Lal, V. P. Gurupur, and P. U. P. Saxena, "Multi-modal medical image fusion with adaptive weighted combination of NSST bands using chaotic grey wolf optimization," *IEEE Access*, vol. 7, pp. 40782–40796, 2019.

[13] S. Das and M. K. Kundu, "NSCT-based multimodal medical image fusion using pulse-coupled neural network and modified spatial frequency," *Med. Biol. Eng. Comput.*, vol. 50, no. 10, pp. 1105–1114, Oct. 2012.

[14] C. X. Huang, G. Tian, Y. Lan, Y. Peng, E. Y. K. Ng, Y. Hao, Y. Cheng, and W. Che, "A new pulse coupled neural network (PCNN) for brain medical image fusion empowered by shuffled frog leaping algorithm," *Frontiers Neurosci.*, vol. 13, pp. 1–10, Mar. 2019.

[15] X. Jin, G. Chen, J. Hou, Q. Jiang, D. Zhou, and S. Yao, "Multimodal sensor medical image fusion based on nonsubsampled shearlet transform and S-PCNNs in HSV space," *Signal Process.*, vol. 153, pp. 379–395, Dec. 2018.

[16] M. Yin, X. Liu, Y. Liu, and X. Chen, "Medical image fusion with parameter-adaptive pulse coupled neural network in nonsubsampled shearlet transform domain," *IEEE Trans. Instrum. Meas.*, vol. 68, no. 1, pp. 49–64, Jan. 2019.

[17] L. Tang, C. Tian, J. Qian, and L. Li, "No reference quality evaluation of medical image fusion," *Int. J. Imag. Syst. Technol.*, vol. 28, no. 4, pp. 267–273, Dec. 2018.

[18] Z. Wang, Y. Ma, F. Cheng, and L. Yang, "Review of pulse-coupled neural networks," *Image Vis. Comput.*, vol. 28, no. 1, pp. 5–13, Jan. 2010.

[19] W.-T. Pan, "A new fruit fly optimization algorithm: Taking the financial distress model as an example," *Knowl.-Based Syst.*, vol. 26, pp. 69–74, Feb. 2012.

[20] W.-T. Pan, "Using modified fruit fly optimisation algorithm to perform the function test and case studies," *Connection Sci.*, vol. 25, nos. 2–3, pp. 151–160, Jun. 2013.

[21] X. Yuan, X. Dai, J. Zhao, and Q. He, "On a novel multi-swarm fruit fly optimization algorithm and its application," *Appl. Math. Comput.*, vol. 233, pp. 260–271, May 2014.

[22] K. Gu, G. Zhai, X. Yang, and W. Zhang, "Using free energy principle for blind image quality assessment," *IEEE Trans. Multimedia*, vol. 17, no. 1, pp. 50–63, Jan. 2015.

[23] K. Gu, J. Zhou, J.-F. Qiao, G. Zhai, W. Lin, and A. C. Bovik, "No-reference quality assessment of screen content pictures," *IEEE Trans. Image Process.*, vol. 26, no. 8, pp. 4005–4018, Aug. 2017.

[24] K. Gu, D. Tao, J.-F. Qiao, and W. Lin, "Learning a no-reference quality assessment model of enhanced images with big data," *IEEE Trans. Neural Netw. Learn. Syst.*, vol. 29, no. 4, pp. 1301–1313, Apr. 2018.

[25] Y. Liu, X. Chen, J. Cheng, and H. Peng, "A medical image fusion method based on convolutional neural networks," in *Proc. 20th Int. Conf. Inf. Fusion*, Jul. 2017, pp. 1–7.

[26] Y. Liu, X. Chen, R. K. Ward, and Z. J. Wang, "Image fusion with convolutional sparse representation," *IEEE Signal Process. Lett.*, vol. 23, no. 12, pp. 1882–1886, Dec. 2016.

[27] S. Li, X. Kang, and J. Hu, "Image fusion with guided filtering," *IEEE Trans. Image Process.*, vol. 22, no. 7, pp. 2864–2875, Jul. 2013.

[28] Y. Liu, S. Liu, and Z. Wang, "A general framework for image fusion based on multi-scale transform and sparse representation," *Inf. Fusion*, vol. 24, pp. 147–164, Jul. 2015.

[29] J. Du, W. Li, B. Xiao, and Q. Nawaz, "Union Laplacian pyramid with multiple features for medical image fusion," *Neurocomputing*, vol. 194, pp. 326–339, Jun. 2016.

[30] S. Das and M. K. Kundu, "A neuro-fuzzy approach for medical image fusion," *IEEE Trans. Biomed. Eng.*, vol. 60, no. 12, pp. 3347–3353, Dec. 2013.

[31] J. Du, W. Li, and B. Xiao, "Anatomical-functional image fusion by information of interest in local Laplacian filtering domain," *IEEE Trans. Image Process.*, vol. 26, no. 12, pp. 5855–5866, Dec. 2017.

[32] J. Du, W. Li, and B. Xiao, "Fusion of anatomical and functional images using parallel saliency features," *Inf. Sci.*, vols. 430–431, pp. 567–576, Mar. 2018.

[33] G. Qu, D. Zhang, and P. Yan, "Information measure for performance of image fusion," *Electron. Lett.*, vol. 38, no. 7, pp. 313–315, Mar. 2002.

[34] C. S. Xydeas and V. Petrović, "Objective image fusion performance measure," *Electron. Lett.*, vol. 36, no. 4, pp. 308–309, Feb. 2000.

[35] C. Yang, J.-Q. Zhang, X.-R. Wang, and X. Liu, "A novel similarity based quality metric for image fusion," *Inf. Fusion*, vol. 9, no. 2, pp. 156–160, Apr. 2008.

CHUANGENG TIAN received the B.S. degree from Hangzhou Dianzi University, in 2005, and the M.S. and Ph.D. degrees from the China University of Mining and Technology, in 2009 and 2017, respectively. He is currently an Associate Professor with the School of Information and Electrical Engineering, Xuzhou University of Technology. His research interests include signal processing, image-based biomedical applications, and wireless sensor networks.

LU TANG received the M.S. and Ph.D. degrees from the China University of Mining and Technology, in 2009 and 2018, respectively. Since 2009, she has been a Teacher with the School of Medical Imaging, Xuzhou Medical University. She currently holds a postdoctoral position with the Department of Radiology, Affiliated Hospital of Xuzhou Medical University. Her research interests include image processing, signal processing, and image-based biomedical applications.

KAI XU received the B.S. degree from Xuzhou Medical University, in 1983, the M.S. degree from the Fourth Military Medical University, in 1990, and the Ph.D. degree from Fudan University, in 2005. He is currently a Professor with Xuzhou Medical University, and the Director of the Department of Radiology, Affiliated Hospital of Xuzhou Medical University. His research interests include the diagnosis of CT and MRI, neuroradiology, and image-based biomedical applications.

• • •